RSC Advances

PAPER

View Article Online
View Journal | View Issue

Cite this: *RSC Adv.*, 2014, **4**, 11967

Linear and nonlinear optical properties for AA and AB stacking of carbon nitride polymorph (C_3N_4)

A. H. Reshak,[ab] Saleem Ayaz Khan*[a] and S. Auluck[c]

The linear and nonlinear optical susceptibilities of AA and AB stacking of the carbon nitride polymorph were calculated using the all electron full potential linear augmented plane wave method based on density functional theory. The complex part of the dielectric function is calculated using the recently modified Becke and Johnson (mBJ) approximation which gives a better optical gap in comparison to the Ceperley–Alder (CA) local density approximation, the *Perdew–Burke–Ernzerhof* generalized gradient approximation, and the Engel–Vosko generalized gradient approximation. The complex dielectric function and other optical constants like refractive index, absorption coefficient, reflectivity and energy loss function are calculated and discussed in detail. The calculated uniaxial anisotropy (−1.06 and −1.04) gives a maximum value of birefringence (−0.89 and −0.87) which increases the suitability of both AA and AB stacking for a large second harmonic generation. The calculated second order susceptibility tensor components $|\chi^{(2)}_{333}(\omega)|$ at the static limit are 19.4 pm V^{-1} and 59.6 pm V^{-1} for AA and AB stacking which increases to 34.2 pm V^{-1} and 106.7 pm V^{-1} at $\lambda = 1064$ nm. The first hyperpolarizability $\beta_{333}(\omega)$ for AA and AB stacking C_3N_4 for the dominant component $|\chi^{(2)}_{333}(\omega)|$ at the static limit are calculated to be (1.6×10^{-30} esu and 9.6×10^{-30} esu) respectively.

Received 14th January 2014
Accepted 17th February 2014

DOI: 10.1039/c4ra00388h

www.rsc.org/advances

1. Introduction

The carbon nitride polymorph (C_3N_4), which comprises covalent bonds, has recently received much interest as a promising material in various applications, for instance as a photocatalyst, fuel cell electrode, light emitting apparatus and chemical sensor. In the past, Liu and Cohen[1] have predicted that β-C_3N_4 has compressibility comparable to that of diamond. The search for the distinct structure of C_3N_4 has a long history. Teter and Hemley[2] studied five types of C_3N_4, including α-C_3N_4, β-C_3N_4, cubic-C_3N_4, pseudocubic-C_3N_4 and graphitic C_3N_4. Their computed results forecast that α-C_3N_4 and graphitic allotropes are energetically highly favored compared to β-C_3N_4. Since then, much effort has been made for the synthesis of C_3N_4. All sorts of methods have been utilized. These include vapor deposition, laser ablation and high pressure high-temperature procedures.[3–5] Due to the chemical inertness of C_3N_4, organizing dense C_3N_4 phases with large crystalline dimensions for explicit characterization is intricate. The g-C_3N_4 preparation has been described.[6–19] A hypothetical material, C_3N_4 may have rather smaller bulk modulus than that of diamond as proposed by first-principles calculations.[20,21] These outcomes have inspired theoretical calculations[22–26] and experimental efforts to synthesize and distinguish this compound.[27–38] From the synthesis of amorphous C–N films,[30,32,36] small crystallites have been discovered in some of these films.[31,33–35] C_3N_4 is a chemically stable compound having a good thermal hardness and astonishing optical characteristics that make it suitable as a photocatalyst under visible light. The pursuit of C_3N_4 has potential for introducing new materials with band gap in the 2.6–3.0 eV range for energy, solar, and LED materials. However, it is important to note the recent advances in the fields of InGaN and AlInN alloy have been widely implemented in solar cells,[39,40] thermoelectricity,[41,42] and LEDs.[43–47]

Wang *et al.*[48] showed that in comparison with other oxides, g-C_3N_4 (having band gap of 2.7 eV) is metal free photocatalyst which can absorb more visible light and produce hydrogen from water. Tahir *et al.*[49] synthesized the tubular g-C_3N_4 and investigated the electrochemical properties which suggest it to be a good contestant for a supercapacitor and photocatalyst used for cleaning environment and energy storage purpose. Recently Wang *et al.*[50] synthesized the nanotube g-C_3N_4 material and demonstrated the intense fluorescence with a photoluminescent, reflecting the applications as a blue light fluorescence material. This material also demonstrates the fabulous visible-light photocatalytic activity, suggesting the high usefulness of g-C_3N_4 nanotubes for gas storage, photocatalysis and light-emitting devices.[50]

From above we notice that there is dearth of theoretical calculations for these materials. There exists a theoretical work

[a]*New Technologies – Research Center, University of West Bohemia, Univerzitni 8, 306 14 Pilsen, Czech republic. E-mail: maalidph@yahoo.co.uk; sayaz_usb@yahoo.com; Tel: +420 777 729 583*

[b]*Center of Excellence Geopolymer and Green Technology, School of Material Engineering, University Malaysia Perlis, 01007 Kangar, Perlis, Malaysia*

[c]*Council of Scientific and Industrial Research – National Physical Laboratory, Dr. K S, Krishnan Marg, New Delhi 110012, India*

based on the pseudopotential method which deals only with valence electrons. Moreover the LDA-CA and GGA-PBE are also not much promising due to their band gap underestimation. It is well-known that the linear and nonlinear optical properties are very sensitive the band gap. Thus calculating the linear and nonlinear optical susceptibilities demands a very accurate energy gap value which should be very close to the experimental value. In our previous work[51] we have calculated the electronic band structure, effective mass and valence electron charge density of AA and AB stacking of C_3N_4. Therefore as a natural extension we think it would be interesting to calculate the linear and nonlinear optical properties of AA and AB stacking of C_3N_4 using an all electron full potential linear augmented plane wave (FPLAPW) method which has proven to be the most precise technique within DFT to calculate the electronic structure of solids.[52,53] In order to explore the effect of different exchange correlation potentials we have performed calculations for four type of exchange and correlation potentials. Thus, based on our previous experiences with this approach, we expect to get more accurate results as compared to the pseudopotential method.

2. Crystal structure and computational details

The crystal structure of AA and AB stacking of C_3N_4 polymorphs is stable in hexagonal symmetry having space group $P\bar{6}m2$. The crystallographic data of C_3N_4 polymorphs are taken from Teter and Hemley.[2] The crystal structure of AA and AB stacking are shown in Fig. 1(a) and (b). We have employed the full potential linear augmented plane wave (FPLAPW) within Wien2k package.[54] Four schemes namely Ceperley–Alder (CA) local density approximation (LDA-CA),[55] *Perdew–Burke–Ernzerhof* generalized gradient approximation (PBE-GGA),[56] Engel–Vosko generalized gradient approximation (EV-GGA)[57] and a recent modified Becke and Johnson (mBJ) scheme[58] were used for the self-consistent calculations. The convergence parameters ($R_{MT}K_{max}$) that used to control size of the basis set for present calculation is set to be 7.0. The expression R_{MT} represent muffin-tin (MT) sphere radius and K_{max} symbolize the magnitude of largest K vector in plane wave expansion. The selected muffin-tin (MT) sphere radii for C and N is 1.24 atomic units (a.u.) in both AA and AB stacking of C_3N_4 polymorphs. The wave function inside the MT sphere was expended up to $l_{max} = 10$ whereas the Fourier expansion of the charge density was expanded up to $G_{max} = 12$ (a.u.)$^{-1}$. The cutoff energy was selected as 6.0 Ryd. The convergence of self consistent calculations was done when the difference in total energy of the crystal did not exceed 10^{-5} Ryd for succeeding steps. The self consistent calculations were obtained for both cases by 308 k points in irreducible Brillouin zone (IBZ).

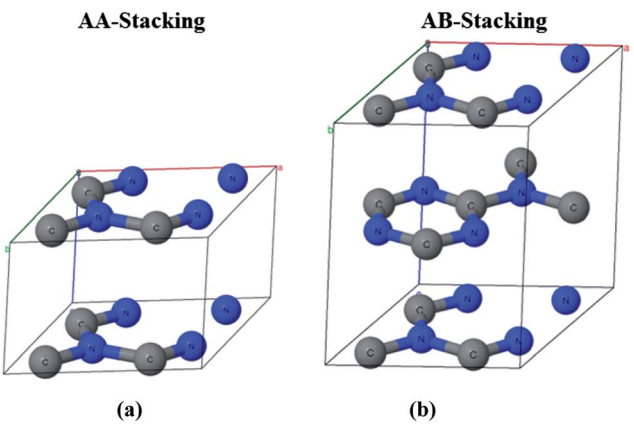

Fig. 1 Crystal structure of C_3N_4 (a) AA-stacking (b) AB-stacking.

3. Result and discussions

3.1. Linear optical properties

The complex dielectric function $\varepsilon(\omega)$ of the material is linked to the energy band structure. The overall band behavior of a solid can be explained by optical spectroscopy analysis of $\varepsilon(\omega)$.[59] The complex dielectric function $\varepsilon(\omega) = \varepsilon_1(\omega) + i\varepsilon_2(\omega)$ is the keynote factor for calculating the optical properties of the materials.[60] The dispersion of dielectric function contains intra- and inter-band transitions. The intra-band transitions are present only in metals. In semiconductors only the inter-band transitions are present. Further the inter-band transitions are divided into direct and indirect band transitions. The contribution of the phonons associated from lattice vibration in indirect inter-band transition are ignored because of small the contribution and only direct band to band transition of electron are taken into account. The correct energy eigenvalues and electron wave functions are necessary to calculate the dispersion of dielectric function $\varepsilon(\omega)$. These are natural output of the band structure calculation. The crystal structure symmetry (hexagonal) of AA and AB stacking of C_3N_4 contains two non-zero principal diagonal dielectric tensor components $\varepsilon^{xx}(\omega) = \varepsilon^{yy}(\omega)$ and $\varepsilon^{zz}(\omega)$ along a, b and c crystallographic axis. These are required to complete the explanation of the linear optical properties. These components can be calculated using the expression taken from ref. 61;

$$\varepsilon_2^{ij} = \frac{4\pi^2 e^2}{Vm^2\omega^2} \times \sum_{nn'\sigma} \langle kn\sigma|p_i|kn'\sigma\rangle\langle kn'\sigma|p_j|kn\sigma\rangle \times f_{kn}(1 - f_{kn'})\delta(E_{kn'} - E_{kn} - \hbar\omega) \quad (1)$$

where m and e represent mass and charge of electron, respectively and ω stands for electromagnetic radiation interacting with the crystal, V stands for unit cell volume, The p notation in bracket represent the momentum operator, $|kn\sigma\rangle$ stand for the crystal wave function with crystal momentum k, and σ spin symbolize the eigenvalue E_{kn}. The Fermi distribution function (f_{kn}) makes sure the counting of transition from occupied to unoccupied state and $\delta(E_{kn'} - E_{kn} - \hbar\omega)$ shows the condition for conservation of total energy.

The structures in the optical response are caused by the electric-dipole transitions between the valence and the conduction bands. In order to identify these structures we need to look at the magnitude of the optical matrix elements. The observed structures would correspond to those transitions that have large optical matrix elements. The calculated absorptive

and dispersive part of AA and AB stacking of C_3N_4 by LDA, GGA-PBE, EVGGA and mBJ, are shown in Fig. 2(a)–(d). This elucidates that mBJ approach shows a better optical gap compared to LDA, GGA and EVGGA. According to our previous experience with mBJ[62–67] we find that mBJ brings the energy gap closer to the experimental one therefore we preferred mBJ scheme for calculations of the linear and nonlinear optical properties as they are very sensitive to the band gap. Fig. 2(e) and (f) shows

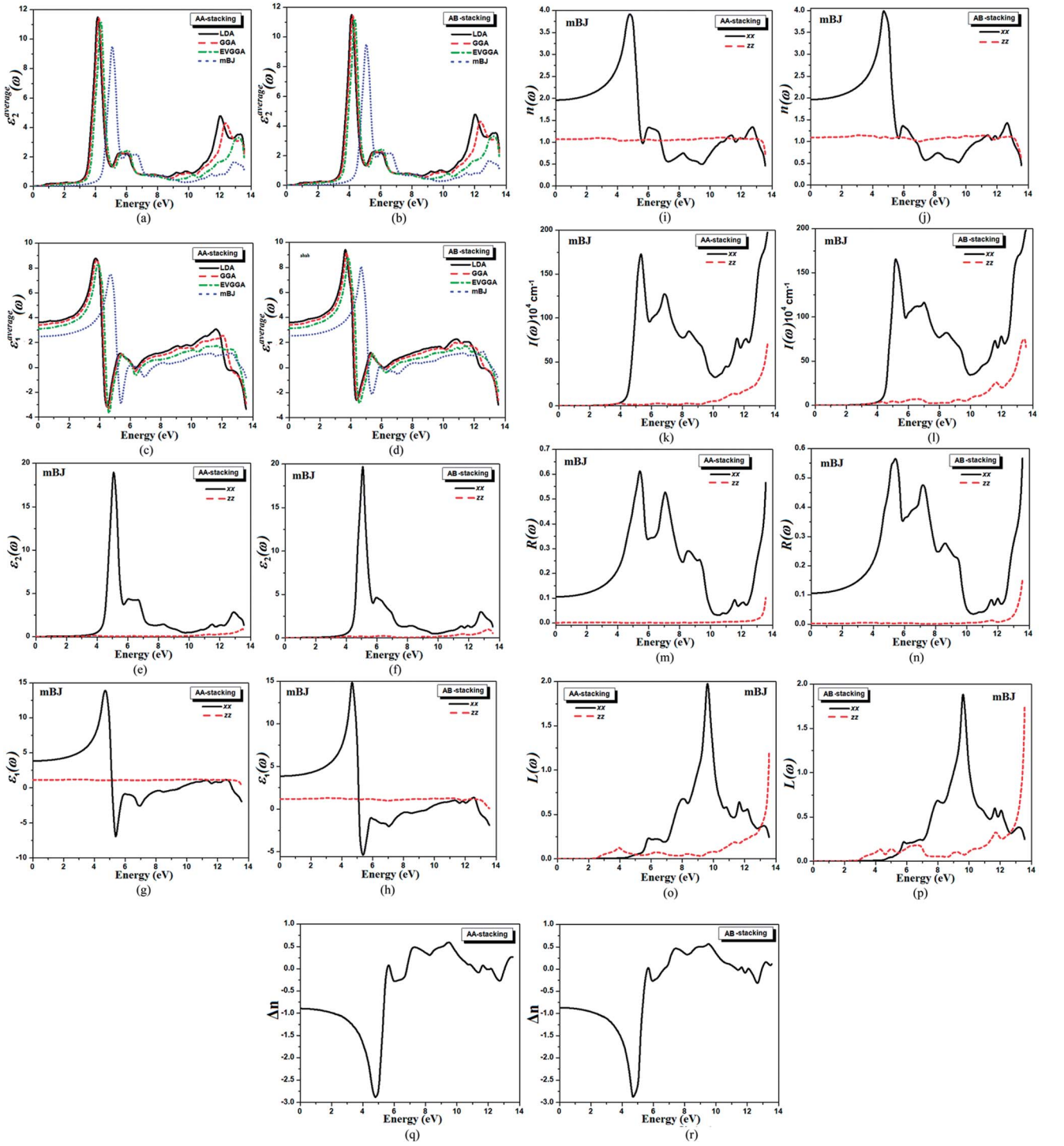

Fig. 2 (a) Calculated $\varepsilon_2^{av}(\omega)$ for AA-stacking C_3N_4; (b) calculated $\varepsilon_2^{av}(\omega)$ for AB-stacking C_3N_4; (c) calculated $\varepsilon_1^{av}(\omega)$ for AA-stacking C_3N_4; (d) calculated $\varepsilon_1^{av}(\omega)$ for AB-stacking C_3N_4; (e) calculated $\varepsilon_2^{xx}(\omega)$ and $\varepsilon_2^{zz}(\omega)$ for AA-stacking; (f) calculated $\varepsilon_2^{xx}(\omega)$ and $\varepsilon_2^{zz}(\omega)$ for AB-stacking; (g) calculated $\varepsilon_1^{xx}(\omega)$ and $\varepsilon_1^{zz}(\omega)$ AA-stacking C_3N_4; (h) calculated $\varepsilon_1^{xx}(\omega)$ and $\varepsilon_1^{zz}(\omega)$ AB-stacking C_3N_4; (i) calculated $n^{xx}(\omega)$ and $n^{zz}(\omega)$ for for AA-stacking; (j) calculated $n^{xx}(\omega)$ and $n^{zz}(\omega)$ for AB-stacking; (k) calculated $I^{xx}(\omega)$ and $I^{zz}(\omega)$ for AA-stacking; (l) calculated $I^{xx}(\omega)$ and $I^{zz}(\omega)$ for AB-stacking; (m) calculated $R^{xx}(\omega)$ and $R^{zz}(\omega)$ for AA-stacking; (n) calculated $R^{xx}(\omega)$ and $R^{zz}(\omega)$ for AB-stacking; (o) calculated $L^{xx}(\omega)$ and $L^{zz}(\omega)$ for AA-stacking; (p) calculated $L^{xx}(\omega)$ and $L^{zz}(\omega)$ for AB-stacking; (q) calculated birefringence (Δn) for AA-stacking; (r) calculated birefringence (Δn) for AB-stacking.

the imaginary part of optical dielectric tensor components for AA and AB stacking of C_3N_4. The calculated $\varepsilon_2(\omega)$ for AA stacking shows a high transparency optical gap up to 2.59 eV while for AB stacking the transparency region increases to 2.99 eV. The first peak in both cases represents transition of electron from valence band maximum to conduction band minimum. Similarly the rest of the peaks represents transitions of electrons from lower occupied bands to upper unoccupied bands. There is a considerable anisotropy between $\varepsilon_2^{xx}(\omega)$ and $\varepsilon_2^{zz}(\omega)$ for whole energy range of AA and AB stacking of C_3N_4. The real part of the optical dielectric tensor components is linked to the electric polarizability of the material which can be calculated from imaginary part using Kramers–Kronig relation;[68]

$$\varepsilon_1(\omega) = 1 + \frac{2}{\pi} P \int_0^{\infty} \frac{\omega' \varepsilon_2(\omega')}{\omega'^2 - \omega^2} \mathrm{d}\omega' \quad (2)$$

Fig. 2(g) and (h) represents the real part of dielectric tensor components for AA- and AB-stacking. The calculated uniaxial anisotropy $\delta\varepsilon = [(\varepsilon_0^{zz} - \varepsilon_0^{xx})/\varepsilon_0^{tot}]$ presented in Table 1, indicates considerable anisotropy[69] between the spectral components of the dielectric function of AA and AB stacking. Table 1 also elucidates the other optical parameters of AA and AB stacking of C_3N_4 in comparison with diamond, β-C_3N_4, α-C_3N_4, γ-C_3N_4 and pc-C_3N_4. Fig. 2(i) and (j) shows the calculated refractive index $n(\omega)$ of AA and AB stacking. The refractive index is also related to the electric polarizability of the material. The static value of refractive index for two non-zero tensor components of AA and AB stacking are directly linked to $n(0)$ by the relation $n(\omega) = \sqrt{\varepsilon_1(0)}$, as shown in Table 1. The most responsible component which increases the refractive index of C_3N_4 is $n^{xx}(\omega)$ while $n^{zz}(\omega)$ shows a negligible role in both stacking cases. When the energy of electromagnetic (EM) waves is increased the $n^{xx}(\omega)$ also increases and achieves a maximum value at 4.9 and 4.8 eV for AA and AB stacking, respectively. Further increasing the energy cause sharp decrease in $n^{xx}(\omega)$. The $n^{xx}(\omega)$ curve crosses the unity at 5.5 eV. This shows the high luminescent nature of AA stacking as compared AB stacking.

The absorption coefficient of the two dielectric tensor components shows a considerable anisotropy between the two components $I^{xx}(\omega)$ and $I^{zz}(\omega)$ for both AA and AB stacking. For both, $I^{xx}(\omega)$ shows dominancy while $I^{zz}(\omega)$ exhibits a minor role. In AA stacking of C_3N_4, the first peak of $I^{xx}(\omega)$ shows maximum absorption of about 175×10^4 cm^{-1} around 5.4 eV, while in AB-stacking the first peak of $I^{xx}(\omega)$ shifts to 5.2 eV with a smaller value of absorption coefficient (167×10^4 cm^{-1}) as shown in Fig. 2(k) and (l). The two components of the reflectivity $R^{xx}(\omega)$ and $R^{zz}(\omega)$ also shows considerable anisotropy. $R^{xx}(\omega)$ plays a leading role with maximum reflection of 62% (AA stacking) and 56% (AB stacking) around 5.5 eV whereas $R^{zz}(\omega)$ shows a negligible role except in the higher energy range (13.5 eV) as shown in Fig. 2(m) and (n).

The energy loss spectrum is related to the energy loss of a fast moving electron in the crystal. Fig. 2(o) and (p) elucidates considerable anisotropy between $L^{xx}(\omega)$ and $L^{zz}(\omega)$ in AA and AB stacking of C_3N_4. In the energy range between 2.59 eV and 5.0 eV for AA stacking and from 2.99 eV to 4.60 eV in AB stacking, $L^{zz}(\omega)$ is the dominant component. As one moves to higher energy range $L^{xx}(\omega)$ becomes dominant in both stacking by showing maximum value of energy loss spectrum around 9.5 eV.

The calculated birefringence $\Delta n(\omega)$ of AA and AB stacking of C_3N_4 polymorph are shown in Fig. 2(q) and (r). Birefringence is given by the relation

$$\Delta n = n_e - n_o$$

where n_e and n_o are the refractive indices categorized in extraordinary and ordinary ray of polarized light. $\Delta n(\omega)$ is very important in the non-absorbing region below the gap.[70] The calculated static values of $\Delta n(\omega)$ are shown Table 1.

3.2. Nonlinear optical properties

The present compounds have only one independent dominant tensor components $\chi^{(2)}_{333}(-2\omega;\ \omega;\ \omega)$. The number in the subscript represents the three polarization directions along x, y and z direction. The first order response only deals with inter-band transitions and involves the square matrix elements giving positive values for $\varepsilon_2(\omega)$. The second harmonic generation (SHG) involves 2ω resonance in accumulation with 1ω resonance which are furthermore separated into inter-band $\chi^{(2)}_{inter}(-2\omega;\ \omega;\ \omega)$, intra-band $\chi^{(2)}_{intra}(-2\omega;\ \omega;\ \omega)$ term along with modulation of intra-band on inter-band term $\chi^{(2)}_{mod}(-2\omega;\ \omega;\ \omega)$. The expressions

Table 1 Calculated linear and non linear optical constants of C_3N_4

	Graphitic-C_3N_4 (AA stacking)	Graphitic-C_3N_4 (AB stacking)	Diamond	β-C_3N_4	α-C_3N_4	γ-C_3N_4	pc-C_3N_4
Space group	$P6\bar{2}m$	$P6\bar{2}m$	$Fd\bar{3}m$	$P6_3/m$	$P3_1c$	$Fd\bar{3}m$	$P4\bar{2}m$
Volume (Å^3)	73.8[a]	147.1[a]	44.2[b]	85.49[b]	170.63[b]	307.91[b]	40.52[b]
E_g (eV)	2.59[a]	2.99[a]	5.72[b], 5.47[c]	3.825[b]	4.672[b]	1.445[b]	2.843[b]
$\varepsilon_1^{xx}(0)$	3.86[a]	3.85[a]	5.70[c]	4.533[b]	4.288[b]	6.275[b]	5.190[b]
$\varepsilon_1^{zz}(0)$	1.15[a]	1.18[a]	5.79[b]	4.755[b]	4.296[b]		
$n^{xx}(0)$	1.95[a]	1.96[a]	2.417[d]	2.129[b]	2.071[b]	2.505[b]	2.278[b]
$n^{zz}(0)$	1.06[a]	1.09[a]	2.417[d]	2.181[b]	2.072[b]	2.505[b]	
$\Delta n(0)$	−0.89[a]	−0.87[a]					
$\delta\varepsilon$	−1.06[a]	−1.04[a]					
Density (g cm^{-3})	2.0215[a]	2.0201[a]	3.51[e]	3.57[f]	3.585[g]	2.620[a,h]	3.811[g]

[a] Present work. [b] Theoretical work ref. 26. [c] Experimental work ref. 37. [d] Experimental work ref. 38. [e] Experimental work ref. 77. [f] Experimental work ref. 78. [g] Theoretical work ref. 2. [h] Experimental work ref. 79.

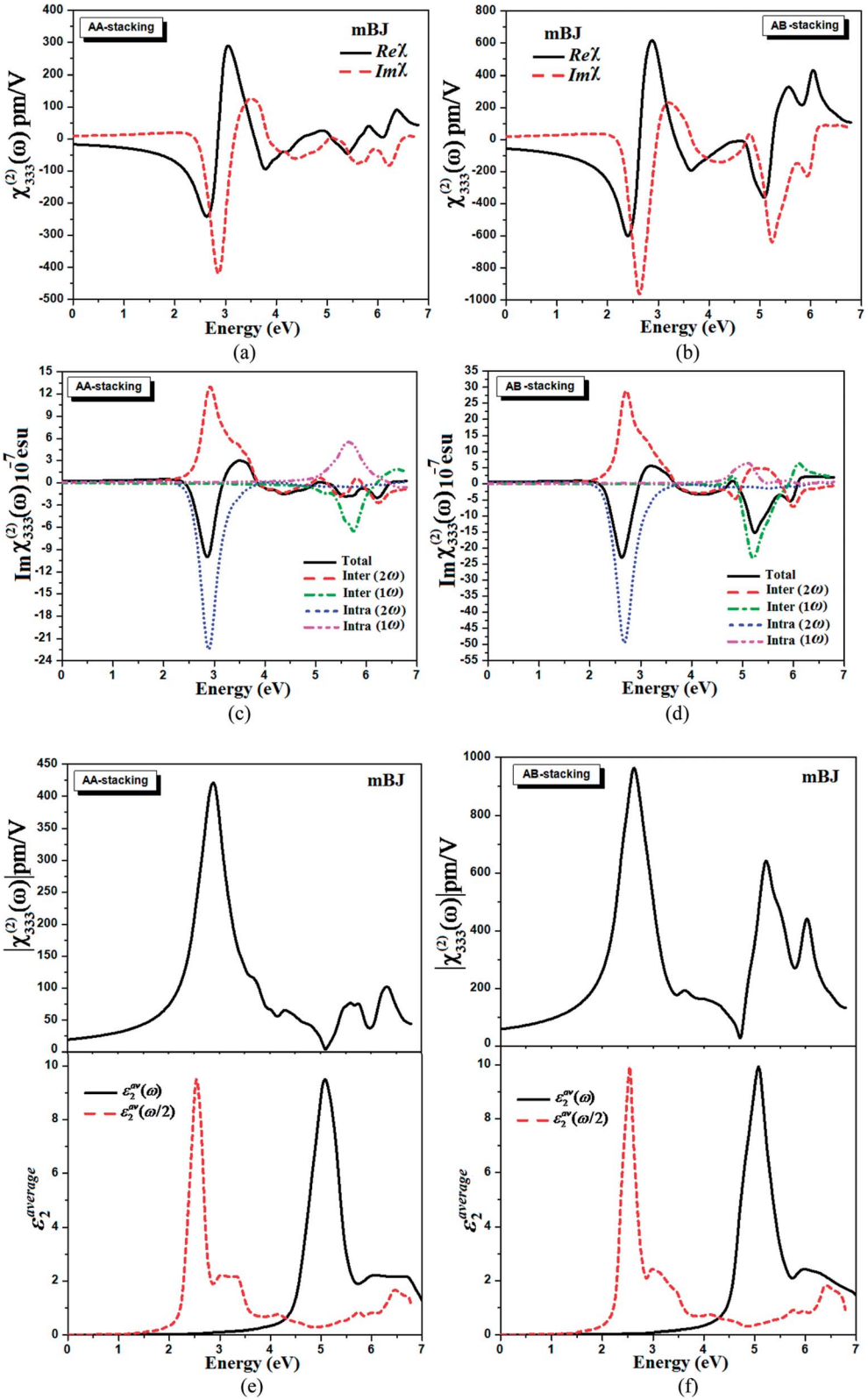

Fig. 3 (a) Calculated real and imaginary of $\chi^{(2)}_{333}(\omega)$ for AA-stacking; (b) calculated real and imaginary of $\chi^{(2)}_{333}(\omega)$ for AB-stacking; (c) calculated total $\mathrm{Im}\chi^{(2)}_{333}(-2\omega;\ \omega;\ \omega)$ along with inter $(2\omega/\omega)$ and intra $(2\omega/\omega)$ band contribution for AA-stacking; (d) calculated total $\mathrm{Im}\chi^{(2)}_{333}(-2\omega;\ \omega;\ \omega)$ along with inter $(2\omega/\omega)$ and intra $(2\omega/\omega)$ band contribution for AB-stacking; (e) calculated $|\chi^{(2)}_{333}(\omega)|$ and $\varepsilon_2^{average}(\omega)$ along with $\varepsilon_2^{average}(\omega/2)$ for AA-stacking; (f) calculated $|\chi^{(2)}_{333}(\omega)|$ and $\varepsilon_2^{average}(\omega)$ along with $\varepsilon_2^{average}(\omega/2)$ for AB-stacking.

Table 2 Calculated nonlinear second order susceptibility and birefringence

	Graphitic-C_3N_4 (AA stacking)	Graphitic-C_3N_4 (AB stacking)	ZnS	GaN	GaAs
$\lvert\chi^{(2)}_{333}(0)\rvert$	19.4[a]	59.6[a]	16.0[b]	6.0[c]	34.0[d]
$\lvert\chi^{(2)}_{333}(\omega)\rvert$	34.2[a]	106.7[a]			
At $\lambda = 1064$ nm					

[a] This work. [b] Experimental work ref. 80. [c] Theoretical work ref. 81. [d] Experimental work ref. 82.

of the complex second-order nonlinear optical susceptibility tensors are given in the ref. 71–75.

Since the nonlinear optical properties are very sensitive to the band gap of the material as compared to linear optical properties therefore, we have selected to show the results obtained by mBJ scheme because it produces better band splitting and hence gives a band gap value close to the experimental one. The importance of the static values of dielectric tensor components of optical susceptibilities cannot be ignored because it is used to calculate the relative frequency of SHG efficiency.[75] The real and imaginary part of second order optical susceptibilities $\chi^{(2)}_{333}$ of both AA and AB stacking of C_3N_4 are shown in Fig. 3(a) and (b). The maximum peak value of $\mathrm{Re}\chi^{(2)}_{333}$ and $\mathrm{Im}\chi^{(2)}_{333}$ for AA stacking are 300 pm V^{-1} and 110 pm V^{-1} which are located at 3.1 eV and 3.5 eV. In AB stacking both peaks shift to 2.8 eV and 3.25 eV with increasing the peak heights to be 610 pm V^{-1} and 215 pm V^{-1} for both $\mathrm{Re}\chi^{(2)}_{333}$ and $\mathrm{Im}\chi^{(2)}_{333}$.

Fig. 3(c) and (d) shows the intra- and inter-band contribution of ω and 2ω resonance for AA and AB stacking of C_3N_4, respectively. One can see that ω resonance is smaller than 2ω resonance in both cases. The maximum peaks of inter- and intra-band of 2ω resonance in AA stacking are located at 2.9 eV which illuminates value of 13×10^{-7} esu and -22.5×10^{-7} esu. For AB stacking these peaks are situated at 2.7 eV with maximum value of 27.5×10^{-7} esu and -49.0×10^{-7} esu for inter- and intra-band contribution of 2ω respectively. Similarly when one moves from AA stacking to AB staking, both contributions (inter- and intra-) of 1ω resonance shifts to lower energy with increasing value of $\mathrm{Im}\chi^{(2)}_{333}$. It is also clear that $\mathrm{Im}\chi^{(2)}_{333}$ shows a zero value below half the band gap ($E_g/2$). The 2ω resonance starts to contribute at energy $> E_g/2$, while ω resonance begins to contribute at energies above E_g. The clear vision of the ω and 2ω resonance can be seen in Fig. 3(e) and (f). The upper panel of Fig. 3(e) and (f) show the calculated value of $\lvert\chi^{(2)}_{333}(\omega)\rvert$ for the dominant tensor component. The value of $\lvert\chi^{(2)}_{333}(\omega)\rvert$ at the static limit $\lvert\chi^{(2)}_{333}(0)\rvert$ is 19.4 pm V^{-1} for AA stacking and 59.6 pm V^{-1} for AB stacking. At $\lambda = 1064$ nm the $\lvert\chi^{(2)}_{333}(\omega)\rvert$ value increased to be 34.2 pm V^{-1} for AA stacking and 106.7 pm V^{-1} for AB stacking.

To analyze the features of the calculated absolute value of the dominant component $\lvert\chi^{(2)}_{333}(\omega)\rvert$ it would be worthwhile helpful to compare $\lvert\chi^{(2)}_{333}(\omega)\rvert$ (Fig. 3(e) and (f) – upper panel) with the absorptive part of the corresponding dielectric function $\varepsilon_2(\omega)$ as a function of both $\omega/2$ and ω (Fig. 3(e) and (f) – lower panel). The 2ω resonance is responsible for spectral structure formation in the energy range from 1.29 eV to 2.59 eV (1.50 eV to 2.99 eV) for AA stacking (AB stacking). The subsequent structure ranges from 2.59 eV to 6.80 eV (2.99 eV to 6.80 eV) for AA stacking (AB stacking) is fashioned by the combined effect of ω and 2ω resonance and the rest of the structure is formed by only ω resonance. The calculated values of second order susceptibility for AA and AB stacking of C_3N_4 are listed in Table 2 in comparison to the experimental and theoretical results of ZnS, GaN and GaAs.

We also have calculated the first hyperpolarizability β_{ijk} vector component along dipole moment direction using the static value of $\lvert\chi^{(2)}_{333}(\omega)\rvert$ and the calculated density for AA stacking and AB stacking (Table 1), using the expression given in ref. 76. The calculated values of $\beta_{333}(\omega)$ are 1.6×10^{-30} esu and 9.6×10^{-30} esu for AA and AB stacking of C_3N_4, respectively.

4. Conclusions

We have calculated the linear and nonlinear optical properties of AA and AB stacking of carbon nitride polymorph using all electron full potential linear augmented plane wave method based on DFT within the frame work of Wien2k code. The exchange correlation energy was solved using four schemes namely Ceperley–Alder (CA) local density approximation, *Perdew–Burke–Ernzerhof* generalized gradient approximation, Engel–Vosko generalized gradient approximation and recent modified Becke and Johnson (mBJ) approximation. We have calculated and discussed in detail the complex dielectric function and the other optical constants such as refractive index, absorption coefficient, reflectivity and energy loss function. The uniaxial anisotropy ($\delta\varepsilon$) was calculated to be -1.06 for AA stacking and -1.04 AB stacking which ensures higher value of birefringence. The value of birefringence at the static limit $\Delta n(0)$ is -0.89 for AA stacking and -0.87 for AB stacking. The values of $\delta\varepsilon$ and $\Delta n(0)$ predict that both AA and AB stacking posses large second harmonic generation. The second order susceptibility tensor components $\lvert\chi^{(2)}_{333}(\omega)\rvert$ for AA-stacking (AB-stacking) were calculated at static limit and at $\lambda = 1064$ nm, these are 19.4 pm V^{-1} and 34.2 pm V^{-1} (59.6 pm V^{-1} and 106.7 pm V^{-1}). In additional we have calculated the first hyperpolarizability $\beta_{333}(\omega)$ using the static value of $\lvert\chi^{(2)}_{333}(\omega)\rvert$. These are 1.6×10^{-30} esu and 9.6×10^{-30} esu for AA and AB stacking of C_3N_4, respectively.

Acknowledgements

The result was developed within the CENTEM project, reg. no. CZ.1.05/2.1.00/03.0088, co-funded by the ERDF as part of the Ministry of Education, Youth and Sports OP RDI programme. SA would like to thank CSIR-NPL for financial assistance.

References

1 A. Y. Liu and M. L. Cohen, *Science*, 1989, **245**, 841–842.
2 D. M. Teter and R. J. Hemley, *Science*, 1996, **271**, 53–55.

3 D. W. He, F. X. Zhang, X. Y. Zhang, Z. C. Qin, M. Zhang, R. P. Liu, *et al.*, *J. Mater. Res.*, 1998, **13**, 3458–3462.
4 Z. Zhang, H. Guo, G. Zhong, F. Yu, Q. Xiong and X. Fan, *Thin Solid Films*, 1999, **346**, 96–99.
5 Y. Peng, T. Ishigaki and S. Horiuchi, *Appl. Phys. Lett.*, 1998, **73**, 3671–3673.
6 V. N. Khabshesku, J. L. Zimmerman and J. L. Margrave, *Chem. Mater.*, 2000, **12**, 3264–3270.
7 M. J. Bojdys, J. O. Muller, M. Antonietti and A. Thomas, *Chem.–Eur. J.*, 2008, **14**, 8177–8182.
8 A. Thomas, A. Fischer, F. Goettmann, M. Antonietti, J. O. Muller, R. Schlogl, *et al.*, *J. Mater. Chem.*, 2008, **18**, 4893–4908.
9 X. Li, J. Zhang, L. Shen, Y. Ma, W. Lei, Q. Cui, *et al.*, *Appl. Phys. A: Mater. Sci. Process.*, 2009, **94**, 387–392.
10 D. R. Miller, J. R. Holst and E. G. Gillan, *Inorg. Chem.*, 2007, **46**, 2767–2774.
11 H. Montigaud, B. Tanguy, G. Demazeau, I. Alves and S. Courjault, *J. Mater. Sci.*, 2000, **35**, 2547–2552.
12 S. M. Lyth, Y. Nabe, S. Moriya, S. Kuroki, M. A. Kakimoto, J. I. Ozaki, *et al.*, *J. Phys. Chem. C*, 2009, **113**, 20148–20151.
13 C. Li, X. G. Yang, B. J. Yang, Y. Yan and Y. T. Qian, *Mater. Chem. Phys.*, 2007, **103**, 427–432.
14 K. Gibson, J. Glaser, E. Milke, M. Marzini, S. Tragl, M. Binnewies, *et al.*, *Mater. Chem. Phys.*, 2008, **112**, 52–56.
15 J. L. Zimmerman, R. Williams, V. N. Khabshesku and J. L. Margrave, *Nano Lett.*, 2001, **1**, 731–734.
16 H. A. Ma, X. P. Jia, L. X. Chen, P. W. Zhu, W. L. Guo, X. B. Guo, *et al.*, *J. Phys.: Condens. Matter*, 2002, **14**, 11269.
17 G. Goglio, D. Andrault, S. Courjault and G. Demazeau, *High Pressure Res.*, 2002, **22**, 535–537.
18 J. Kouvetakis, M. Todd, B. Wilkens, A. Bandari and N. Cave, *Chem. Mater.*, 1994, **6**, 811–814.
19 E. G. Gillan, *Chem. Mater.*, 2000, **12**, 3906–3912.
20 A. Y. Liu and M. L. Cohen, *Science*, 1989, **245**, 841.
21 A. Y. Liu and M. L. Cohen, *Phys. Rev. B: Condens. Matter Mater. Phys.*, 1990, **41**, 10727.
22 J. L. Corkill and M. L. Cohen, *Phys. Rev. B: Condens. Matter Mater. Phys.*, 1993, **48**, 17622.
23 H. Yao and W. Y. Ching, *Phys. Rev. B: Condens. Matter Mater. Phys.*, 1994, **50**, 11231.
24 J. Ortega and O. F. Sankey, *Phys. Rev. B: Condens. Matter Mater. Phys.*, 1995, **51**, 2624.
25 Y. Guo and W. A. Goddard, *Chem. Phys. Lett.*, 1995, **237**, 72.
26 J. Hu, *Appl. Phys. Lett.*, 1995, **89**, 261117.
27 T. Sekine, H. Kanda, Y. Bando, M. Yokohama and K. Hojou, *J. Mater. Sci. Lett.*, 1990, **9**, 1376.
28 L. Maya, D. R. Cole and E. W. Hagaman, *J. Am. Ceram. Soc.*, 1991, **74**, 1686.
29 J. J. Cuomo, P. A. Leary, D. Yu, W. Reuter and M. Frisch, *J. Vac. Sci. Technol.*, 1976, **16**, 299.
30 H. X. Han and B. J. Feldman, *Solid State Commun.*, 1988, **65**, 921.
31 C. Niu, Y. Z. Liu and C. M. Lieber, *Science*, 1993, **261**, 334.
32 D. Marton, K. J. Boyd, A. H. Al-Bayati, S. S. Todorov and J. W. Rablais, *Phys. Rev. Lett.*, 1994, **73**, 118.
33 K. M. Yu, M. L. Cohen, E. E. Haller, W. L. Hansen, A. Y. Lu and I. C. Wu, *Phys. Rev. B: Condens. Matter Mater. Phys.*, 1994, **49**, 5034.
34 J. P. Riviere, D. Texier, J. Delafond, M. Jaouen, E. L. Mathe and J. Chaumont, *Mater. Lett.*, 1995, **22**, 115.
35 Z. M. Ren, *et al.*, *Phys. Rev. B: Condens. Matter Mater. Phys.*, 1995, **51**, 5274.
36 Y. Yang, K. A. Nelson and F. Adibi, *J. Mater. Res.*, 1995, **10**, 41.
37 M. H. V. Huynh, M. A. Hiskey, J. G. Archuleta and E. L. Roemer, *Angew. Chem., Int. Ed.*, 2004, **43**, 5658; 2005, **44**, 737.
38 H. R. Phillip and E. A. Taft, *Phys. Rev.*, 1964, **136**, A1445.
39 E. C. Young, F. Wu, A. E. Romanov, D. A. Haeger, S. Nakamura, S. P. Denbaars, D. A. Cohen and J. S. Speck, *Appl. Phys. Lett.*, 2012, **101**, 5.
40 C. J. Neufeld, N. G. Toledo1, S. C. Cruz, M. Iza, S. P. DenBaars and U. K. Mishra, *Appl. Phys. Lett.*, 2008, **93**, 143502.
41 J. Zhang, H. Tong, G. Liu, J. A. Herbsommer, G. S. Huang and N. Tansu, *J. Appl. Phys.*, 2011, **109**, 053706.
42 J. Zhang, S. Kutlu, G. Liu and N. Tansu, *J. Appl. Phys.*, 2011, **110**, 043710.
43 D. Feezell, *et al.*, *J. Disp. Technol.*, 2013, **9**, 190–198.
44 H. Zhao, G. Liu, J. Zhang, J. D. Poplawsky, V. Dierolf and N. Tansu, *Opt. Express*, 2011, **19**, A991–A1007.
45 R. A. Arif, H. Zhao and N. Tansu, *Appl. Phys. Lett.*, 2008, **92**, 011104.
46 H. Zhaol, R. A. Arif and N. Tansu, *J. Appl. Phys.*, 2008, **104**, 043104.
47 K. T. Delaney, P. Rinke and C. G. Van de Walle, *Appl. Phys. Lett.*, 2009, **94**, 191109.
48 X. C. Wang, K. Maeda, A. Thomas, K. Takanabe, G. Xin, J. M. Carlsson, K. Domen and M. Antonietti, *Nat. Mater.*, 2009, **8**, 76.
49 M. Tahir, C. Cao, F. K. Butt, F. Idrees, N. Mahmood, I. Aslam, Z. Ali, M. Tanvir, M. Rizwan and T. Mahmood, *J. Mater. Chem. A*, 2013, **1**, 13949.
50 S. Wang, C. Li, T. Wang, P. Zhang, A. Li and J. Gong, *J. Mater. Chem. A*, 2014, **2**, 2885.
51 A. H. Reshak, S. A. Khan and S. Auluck, *RSC Adv.*, 2014, **4**, 6957–6964.
52 S. Gao, *Comput. Phys. Commun.*, 2003, **153**, 190–198.
53 K. Schwarz, *J. Solid State Chem.*, 2003, **176**, 319–328.
54 P. Balaha, K. Shewartz, G. K. H. Madsen, D. Kvsnicka and J. Luitz, *WIEN2K, an Augmented plane wave +local orbitals program for calculating crystals properties*, Karlheinz Schewartz, Techn. Universitat, Wien, Austria, 2001, ISBN 3-9501031-1-2.
55 D. M. Ceperley and B. I. Alder, *Phys. Rev. Lett.*, 1980, **45**, 566.
56 J. P. Perdew, K. Burke and M. Ernzerhof, *Phys. Rev. Lett.*, 1996, **77**, 3865.
57 E. Engel and S. H. Vosko, *Phys. Rev. B: Condens. Matter Mater. Phys.*, 1993, **47**, 13164.
58 F. Tran and P. Blaha, *Phys. Rev. Lett.*, 2009, **102**, 226401.
59 S. A. Khan and A. H. Reshak, *Int. J. Electrochem. Sci.*, 2013, **8**, 9459–9473.
60 A. H. Reshak and S. A. Khan, *Comput. Mater. Sci.*, 2013, **78**, 91–97.

61 A. Delin, P. Ravindran, O. Eriksson and J. M. Wills, *Int. J. Quantum Chem.*, 1998, **69**, 349–358.
62 A. H. Reshak, X. Chen, S. Auluck and H. Kamarudin, *Mater. Chem. Phys.*, 2012, **137**, 346–352.
63 A. H. Reshak, X. Chen, S. Auluck and H. Kamarudin, *J. Appl. Phys.*, 2012, **112**, 053526.
64 A. H. Reshak, I. V. Kityk, O. V. Parasiuk, A. O. Fedorchuk, Z. A. Alahmed, N. AlZayed, H. Kamarudin and S. Auluck, *J. Mater. Sci.*, 2013, **48**, 1342–1350.
65 A. H. Reshak, I. V. Kityk, O. V. Parasyuk, H. Kamarudin and S. Auluck, *J. Phys. Chem. B*, 2013, **117**, 2545–2553.
66 M. Benkraouda and N. Amrane, *J Alloys Compd.*, 2013, **546**, 151–156.
67 S. Guo and B. Liu, *J. Magn. Magn. Mater.*, 2012, **324**, 2410–2415.
68 H. Tributsch, *Z. Naturforsch.*, 1977, **32**, 972.
69 A. H. Reshak, X. Chen, S. Auluck and I. V. Kityk, *J. Chem. Phys.*, 2008, **129**, 204111.
70 A. H. Reshak, S. Auluck and I. V. Kityk, *Phys. Rev. B: Condens. Matter Mater. Phys.*, 2007, **75**, 245120.
71 S. Sharma, J. K. Dewhurst and C. Ambrosch-Draxl, *Phys. Rev. B: Condens. Matter Mater. Phys.*, 2003, **67**, 165332.
72 A. H. Reshak, Ph.D. thesis, Indian Institute of Technology-Rookee, India, 2005.
73 A. H. Reshak, *J. Chem. Phys.*, 2006, **125**, 014708.
74 A. H. Reshak, *J. Chem. Phys.*, 2006, **124**, 014707.
75 A. H. Reshak, H. Kamarudin and S. Auluck, *J. Mater. Sci.*, 2013, **48**, 1955–1965.
76 R. W. Boyd, *Nonlinear Optics*, Academic Press is an imprint of Elsevier, ISBN: 978-0-12-369470-6, third edition, 2008
77 J. W. Zou, K. Reichelt, K. Schmidt and B. Dischler, *J. Appl. Phys.*, 1989, **65**, 3914–3918.
78 J. Hu, P. Yang and C. M. Lieber, *Phys. Rev. B.*, 1998, **57**(6), R3185–R3188.
79 L. C. Ming, P. Zinin, Y. Meng, X. R. Liu, S. M. Hong and Y. Xie, *J. Appl. Phys.*, 2006, **99**, 033520.
80 D. T. F. Marple, *J. Appl. Phys.*, 1964, **35**, 539.
81 J. L. P. Hughes, Y. Wang and J. E. Sipe, *Phys. Rev. B: Condens. Matter Mater. Phys.*, 1997, **55**(20), 13630.
82 B. F. Levine and C. G. Bethea, *Appl. Phys. Lett.*, 1972, **20**, 272.

